 doi:10.20944/preprints202209.0372.v1

Article

Magnetic Induced Terahertz Modulation Characteristics based on Ferromagnetic Nematic Liquid Crystals

Qinghao Meng [1, 2, 3, 4], Xueyan Wang [1], Boyan Zhang [1, 2, 3, 4], Siyu Qian [1, 2, 3, 4], Bo Peng [1, 2, 3, 4], Hangyu Zhou [1], Bo Su [1, 2, 3, 4, *] and Cunlin Zhang [1, 2, 3, 4]

[1] Department of Physics, Capital Normal University, Beijing 100048, China
[2] Beijing Key Laboratory for Terahertz Spectroscopy and Imaging, Beijing 100048, China
[3] Beijing Advanced Innovation Centre for Imaging Theory and Technology, Beijing 100048, China
[4] Key Laboratory of Terahertz Optoelectronics, Ministry of Education, Beijing 100048, China
* Corresponding author: subo75@cnu.edu.cn

Abstract: In recent years, solid state terahertz (THz) modulators have obtained rapid progress with the widespread use of two-dimensional (2D) materials in the field of THz; however, challenges remain in preparing flexible THz modulators. In this study, flexible ferromagnetic nematic materials were prepared by doping thermotropic nematic liquid crystals 5CB into magnetic fluids, and the influence of hydrogen bonding in water was reduced by a self-made cyclic olefin copolymer (COC) microfluidic chip. THz modulation characteristics of magnetic fluid and ferromagnetic nematic liquid crystal (FNLC) under the induction of external magnetic field were compared using a THz time domain spectroscopy system. Under the action of a 91 mT magnetic field, the magnetic fluid has a maximum modulation depth (MD) of 54%. Under the same magnetic field, the maximum MD of the FNLC materials increase to 78% because of the rearrangement of Fe_3O_4 nanoparticles induced by the topological defect of the liquid crystal. We demonstrate that the magneto-optical effect is significantly enhanced in the ferromagnetic nematic liquid crystal hybrid system. This strategy of doping thermotropic nematic liquid crystals to enhance the magneto-optical effect has great potential for THz filtering, modulation, and sensing applications.

Keywords: magnetic fluid; thermotropic nematic liquid crystals; terahertz modulation; microfluidic chip

1. Introduction

A terahertz (THz) [1-6] wave is an electromagnetic wave with the frequency range of 0.1–10 THz and the wavelength range of 0.03–3 mm, which is a promising frequency range in the electromagnetic spectrum. In recent times, THz technology have made great progress in basic research fields such as biological diagnosis, medical imaging, and wireless communication [7-11]. Artificial electromagnetic materials, such as photonic crystals (PCs), metamaterials, and plasma elements, have been extensively studied and used to modulate THz waves [12-14]. THz magneto-optical (MO) elements, controlled by an external magnetic field, are integral parts of the field of broadband amplitude modulation [15, 16]. A magnetic fluid is the stable colloidal system composed of nanoscale ferromagnetic particles that are highly homogeneously dispersed in some carrier liquids by surfactants. Magnetic fluid has been used in the field of THz modulation, as a flexible composite functional material because of its excellent MO effect. Shalaby et al. [17] used liquid suspended magnetic nanoparticles (NPs i.e., magnetic fluid) to modulate THz waves at a very low magnetic field. Liu et al. [18] used magnetic fluids and metamaterials to design a multifunctional THz wave modulator. The absorption peak of the metamaterials induced a frequency shift of 33 GHz at low magnetic field intensity, resulting in a THz amplitude modulation depth (MD) of 34%. Magnetic fluids, as flexible colloidal materials, broaden the range of applications for THz modulators, but enhancing their MD becomes an urgent problem.

Preprints (www.preprints.org) | NOT PEER-REVIEWED | Posted: 23 September 2022 doi:10.20944/preprints202209.0372.v1

Liquid crystal is a partially ordered anisotropic fluid, thermodynamically located between the three-dimensional (3D) lattice of solid crystal and a flow controlled isotropic liquid state. The development of liquid crystal photonics devices has gradually extended from short-wave (e.g., visible and near-infrared bands) to long-wave directions (THz band) because of its good broadband optical anisotropy and external field-controllable electro-optical and MO modulation properties. Particularly, the combination of liquid crystal materials with artificial micro-electromagnetic structures (PCs, metamaterials, and nanomaterials) can result in new THz-tunable devices [19, 20]. Chen et al. [21] prepared a THz metamaterial fast-response optical switch embedded with dual-frequency liquid crystal. The dual frequency liquid crystal with the thickness of 50 μm was electrically controlled to produce the frequency tuning range of 15 GHz, and the response times for red-shifting and blue-shifting of the transmission resonance peak were 1.044 and 1.376 ms, respectively. Savo et al. [22] validated a THz spatial light modulator based on the function of metamaterial absorber, achieving an MD of 75% through an electronically controlled liquid crystal. Isić et al. [23] proposed a compact metamaterial absorber with an MD of more than 23 dB, 15% spectral tuning, and a response time of 50 ms. Liquid crystal nanoscience is an emerging area of research. Nanoparticle-doped liquid crystal composites have been developed that have more tunable properties under the application of electricity or magnetic field than conventional nanomaterials. [24].

In this study, THz time domain spectroscopy (THz-TDS) system and microfluidic technique are used to compare the modulation characteristics of THz waves by magnetic fluids and ferromagnetic nematic liquid crystals (FNLC). First, water-based magnetic fluids were doped with thermotropic nematic liquid crystal 5CB, i.e., 4-cyano-4'-pentylbiphenyl, to prepare FNLCs. Then, we designed a microfluidic chip [25] with the detection zone made of cyclic olefin copolymer (COC) material, that is transparent and has no significant absorption peaks in the THz range, in order to reduce the experimental impact of THz wave absorption by hydrogen bonds in water. The THz transmittance of a 2 mm thick COC material exceeded 90% [26] (Figure S1). Finally, the chip was used to research the THz modulation properties of the magnetic fluid and FNLC under an external magnetic field. Both exhibit broadband modulation performance in an effective frequency range (0.3-2.4 THz). The maximum MD of magnetic fluid was 54% under the action of a 91 mT magnetic field and increased to 78% for the FNLC material under the same magnetic field because of the topological defects of the liquid crystal inducing the rearrangement of Fe_3O_4 NPs [27]. We demonstrate that the MO effect in the FMLC hybrid system is significantly enhanced [28].

2. Materials and Methods

2.1. Material preparation

We purchased 5CB (4-cyano-4'-pentylbiphenyl, $C_{18}H_{19}N$, 98%) and magnetic fluid (Fe_3O_4 NPs, 99.5%, particle size 20 nm, hydrophilic) from Macklin. The 5CB molecules are oriented in a homogeneous arrangement, as thermotropic nematic liquid crystals, exhibiting dielectric anisotropy and refractive index anisotropy. The nematic liquid crystal molecules have a rod-shaped structure and orderly orientation, optically shown as uniaxial crystals (Figure S2). In the experiment, the magnetic fluid was first released using deionized water as the dilution solvent. During the dilution process, the sample solution was sonicated for 1 h to make it fully miscible, allowing the magnetic NPs to be uniformly dispersed in the aqueous base solution, and a magnetic fluid sample with a volume fraction of 0.62% was prepared. Following that, 1 mL of nematic liquid crystal 5CB was filled into an empty test tube using a pipette, and 3 mL of the configured magnetic fluid sample was dropped into it using a pipette. Finally, using the small elasticity coefficient and topological defects of the nematic liquid crystal, the sample was again sonicated in an ultrasonic cleaning machine for 1 h using the ultrasonic resonance fusion method, so that the liquid crystal molecules and magnetic particles could be uniformly dispersed in the carrier liquid and exist stably. Finally, FNLC with a volume fraction of 25% and 0.48% for 5CB

Preprints (www.preprints.org) | NOT PEER-REVIEWED | Posted: 23 September 2022 doi:10.20944/preprints202209.0372.v1

and Fe_3O_4 NPs, respectively, were prepared. Note that during the ultrasonic mixing, the water temperature in the machine should be controlled below 40℃ to ensure the quality of the mixed sample solution.

2.2. Experimental devices

The THz-TDS system mainly includes femtosecond laser, time delay control system, THz wave generation device and detection device, with effective bandwidth ranging from 0.3–2.4 THz (as shown in Figure 1). The laser uses a self-locking fiber femtosecond laser (output power: 130 mW, center wavelength: 1,550 nm, pulse repetition rate: 100 MHz, and pulse width: 75 fs). The output laser is divided into pump pulse and detection pulse by using a polarization beam splitting (PBS). The former is coupled to the fiber optic waveguide antenna (BATOP bPCA-100-05-10-1550-x) through the time delay control system for generating THz wave, and the latter is coupled to the fiber optic waveguide antenna (BATOP bPCA-180-05-10-1550-x) for detecting THz wave. In the experiment, the microfluidic chip was fixed between the off-axis parabolic mirrors. The THz waves penetrate the sample-filled chip and are then picked up by the detection antenna and fed into a lock-in amplifier for amplification. Eventually, the computer is used for data processing.

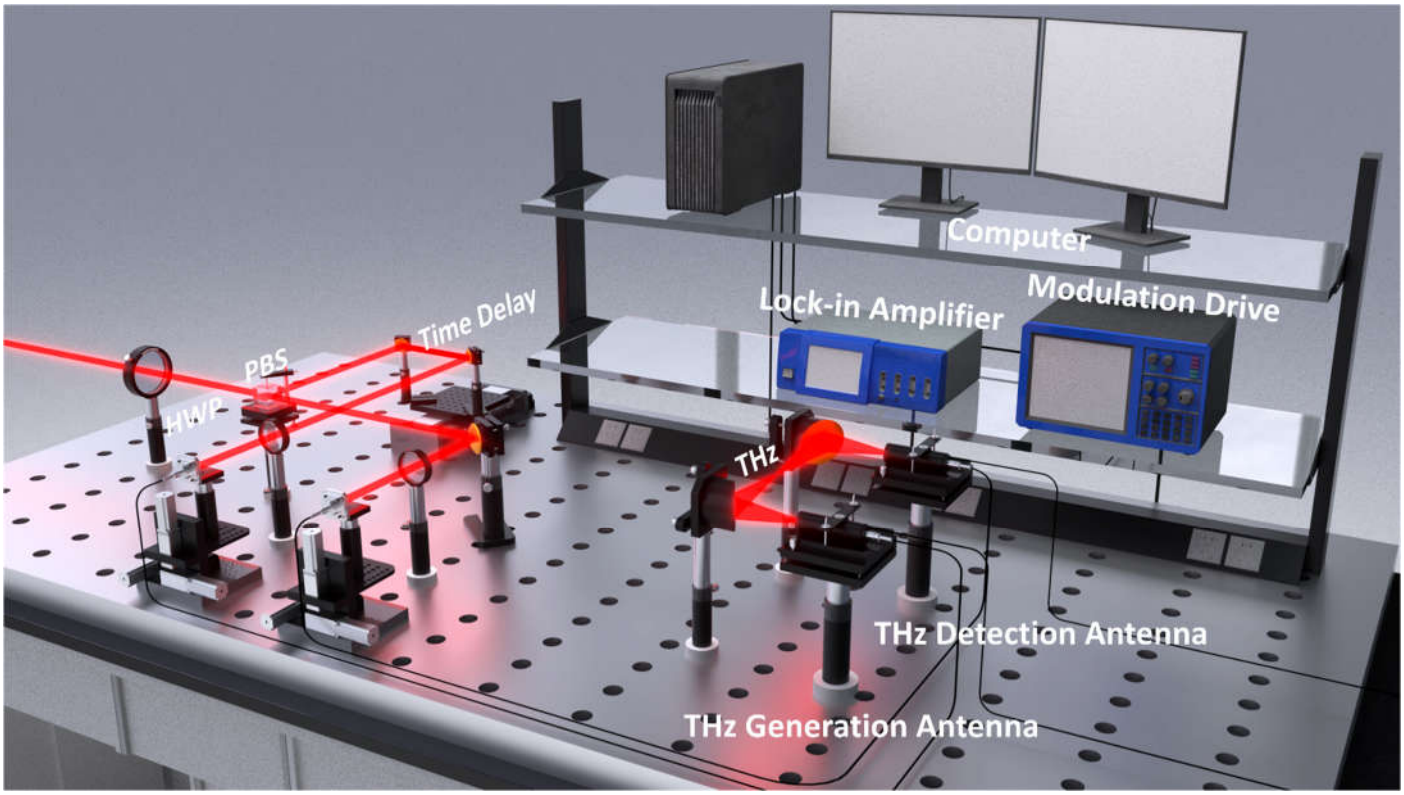

Figure 1. Schematic diagram of the THz-TDS system.

The THz microfluidic chip preparation flow in this study is shown in Figure 2. We used COC material in the probe area of the chip and prepared the rest of the chip using plexiglass (PMMA), due to the fact that sheet COC material is expensive and difficult to obtain. The PMMA was first cut into 20 × 20 × 2 mm^3 sheet using the laser engraver cutting function, and square hole of 10 × 10 × 2 mm^3 was cut in the sample probe area. Next, two cylindrical channels of 5 mm in length and 0.7 mm in diameter were spotted on the left and right sides of the upper side of the PMMA using the laser engraver spotting function, and channels of 0.7 mm in diameter were spotted on the left and right sides of the chip so that they were perpendicular and connected. The COC material is then cut to match the size of the square hole and a 10 × 4 × 0.3 mm^3 sample probe area is milled in the center of the material's side with a milling cutter. Finally, the COC material is embedded in the

Preprints (www.preprints.org) | NOT PEER-REVIEWED | Posted: 23 September 2022 doi:10.20944/preprints202209.0372.v1

PMMA, the two materials and the holes on the left and right sides are sealed with hot melt adhesive to avoid leakage. The upper left inner L-shaped channel of the PMMA is used as the input channel and the upper right inner L-shaped channel is used as the output channel.

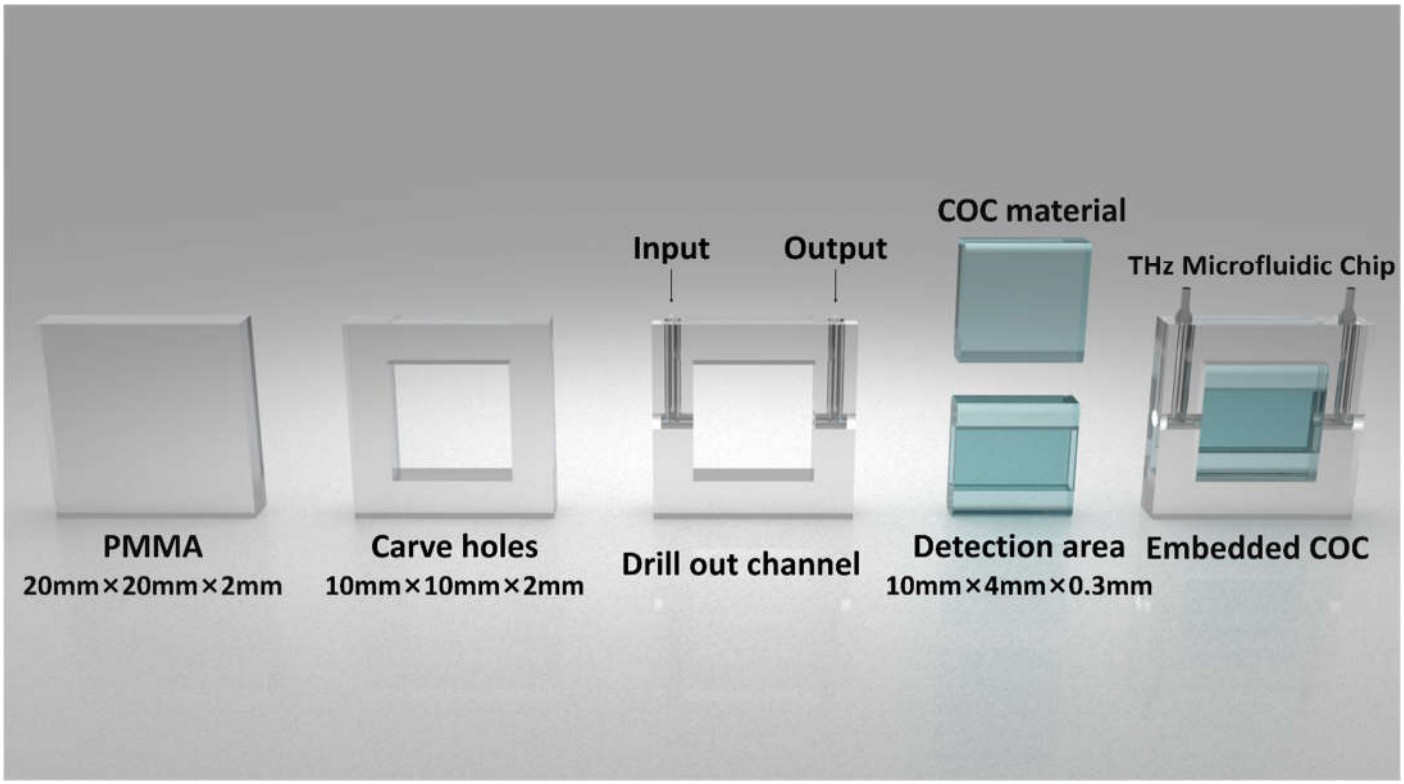

Figure 2. Preparation flowchart of COC-based THz microfluidic chip

2.3. Experimental procedure

The prepared magnetic fluid and FNLC were sequentially injected into a microfluidic chip, which was then placed in the THz-TDS system for the modulation research. The experimental procedure of the magnetic fluid and FNLC modulation is shown in Figure 3. We used a DC circular electromagnet as the magnetic control source in the experiment. By varying the input voltage, the magnetic field intensity around the chip can be adjusted in the range of 0-100 mT. First, a polarizer is used to convert the THz beam into linearly polarized light polarized along the z-axis. Then, the THz modulation characteristics of the magnetic fluid and FNLC were investigated when the magnetic field direction was parallel to the polarization direction (Figure 3 (a)) and orthogonal (Figure 3 (b)) to the polarization direction, as the magnetic field direction induced the magnetic fluid and FNLC to absorb THz waves, resulting in dichroism [29].

 doi:10.20944/preprints202209.0372.v1

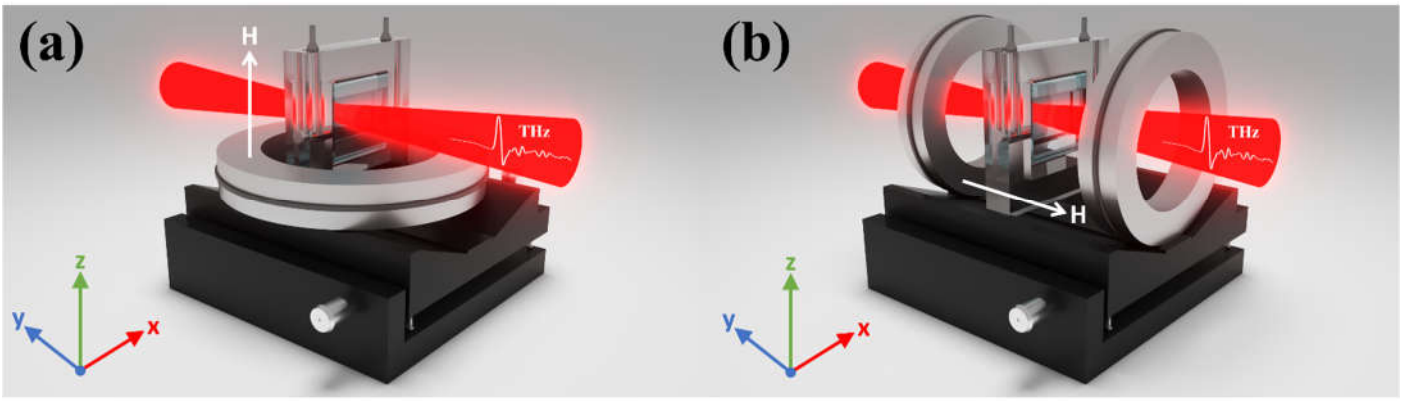

Figure 3. THz wave modulation experiment of magnetic fluid and FNLC when the magnetic field direction is parallel (a) and orthogonal (b) to the THz wave polarization direction.

3. Results

Figure 4 shows the experiment results of the 5CB, magnetic fluid and FNLC modulating THz waves under the action of external magnetic field. In experiment, the electric field of the THz wave is polarized along the z-axis. The ordinary wave propagates with the magnetic field orthogonal to the polarization direction; the extraordinary wave propagates with the magnetic field parallel to the polarization direction. The THz frequency domain spectrum of the extraordinary wave passing through the magnetic fluid and the FNLC under the control of the magnetic field is shown in Figures 4(a) and 4(b), respectively. Figure S3 shows the THz frequency domain spectrum of extraordinary waves passing through 5CB under the control of magnetic field. The transmission amplitude of the THz wave gradually decays as the applied magnetic field strength increases (0, 9, 15, 43, 91 mT). We calculated the curves of MD versus magnetic field strength for the 5CB, magnetic fluid and FNLC at 0.61 THz (Figure 4(c)), and the maximum MD of the magnetic fluid is 54%. After doping the thermotropic nematic liquid crystal 5CB, the maximum MD of the FNLC increases to 78%. We calculated the THz absorption coefficient curves for 5CB, magnetic fluid and FNLC using the flat-plate medium model illustrated in Supporting Information (Figures 4(d), 4(e) and 4(f)) to quantitatively verify the modulation properties of the three materials to THz waves. The absorption of THz wave by three materials increases with the strength of the applied magnetic field, resulting in THz waves modulation properties under the dominate of weak magnetic field. A quantitative comparison of absorption coefficients reveals that doping liquid crystals into the magnetic fluid improves its modulation ability to THz waves under the same magnetic field because the reference signals of the three samples are the same deionized aqueous solution.

Preprints (www.preprints.org) | NOT PEER-REVIEWED | Posted: 23 September 2022 doi:10.20944/preprints202209.0372.v1

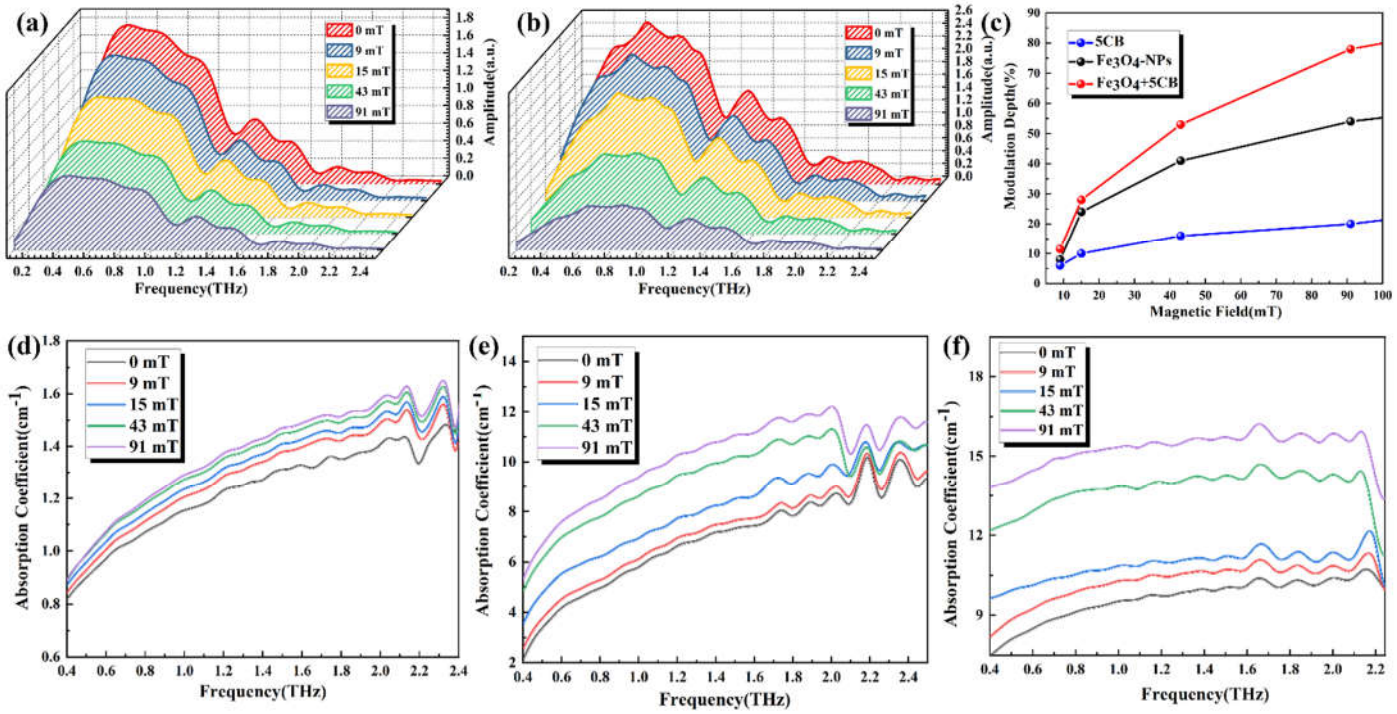

Figure 4. Schematic of comparative experimental results of THz wave modulation by 5CB, magnetic fluid and FNLC. (a) THz frequency domain spectrum of a magnetic fluid at different magnetic field strength. (b) THz frequency domain spectrum of FNLC under different magnetic field strength. (c) MD of 5CB (bule line), magnetic fluid (black line) and FNLC (red line) at 0.61 THz versus external magnetic field strength. (d) THz absorption coefficient diagram of 5CB. (e) THz absorption coefficient diagram of magnetic fluid. (f) THz absorption coefficient diagram of FNLC.

4. Discussion

Magnetic fluid (i.e., Fe_3O_4 NPs), as a good MO material, has significant application prospects in THz sensing and modulation [31,32]. Chen et al. [33] demonstrated the magnetically induced tunability of the in-plane refractive index of Fe_3O_4 NPs. Scholten et al. [34] proved the birefringence effect and linear dichroism in magnetic fluid in 1980. In this research, THz modulation experiment was carried out on the magnetic fluid in the presence of external magnetic field and the experimental result was similar to Shalaby et al [17]. In the absence of an external magnetic field, Fe_3O_4 NPs are randomly oriented to generate a zero magnetic state, and THz waves undergo isotropic absorption. After the application of the magnetic field, the NPs reoriented along the direction of the magnetic field in Neal and Brown types of magnetic moments, forming chain-like clusters. The formation of clusters makes Fe_3O_4 NPs have good linear dichroism, and their absorption of THz waves depends on the angle between magnetic field and THz polarization directions [17, 33-35]. Compared to the isotropic case, the absorption of ordinary wave by the magnetic fluid decreases, and the transmission increases, whereas the absorption of magnetic fluid for the extraordinary waves increases and the transmission decreases (Figure 5(a)). The following three mechanisms explain THz wave attenuation when traversing a magnetic fluid via a magnetic fluid. The first is Rayleigh scattering, which occurs during the formation of clusters in the direction of the magnetic field. It is a tunable characteristics of THz waves under magnetic control caused by structural changes. The second is the virtual component absorption of cluster magnetic polarization, an eddy current loss in colloidal particles by THz waves under the action of external magnetic field. Due to the low macroscopic conductivity between magnetic fluid. The value of the σ_r is stable at approximately 5×10^{-6} S/m (Figure 5(b)). This absorption can be ignored. The third is the virtual

Preprints (www.preprints.org) | NOT PEER-REVIEWED | Posted: 23 September 2022 doi:10.20944/preprints202209.0372.v1

component absorption of cluster electric polarization, which represents the current generated in colloidal NPs. Even in the presence of weak magnetic field, this component will lead to significant attenuation, making it the main mechanism of light absorption in this study.

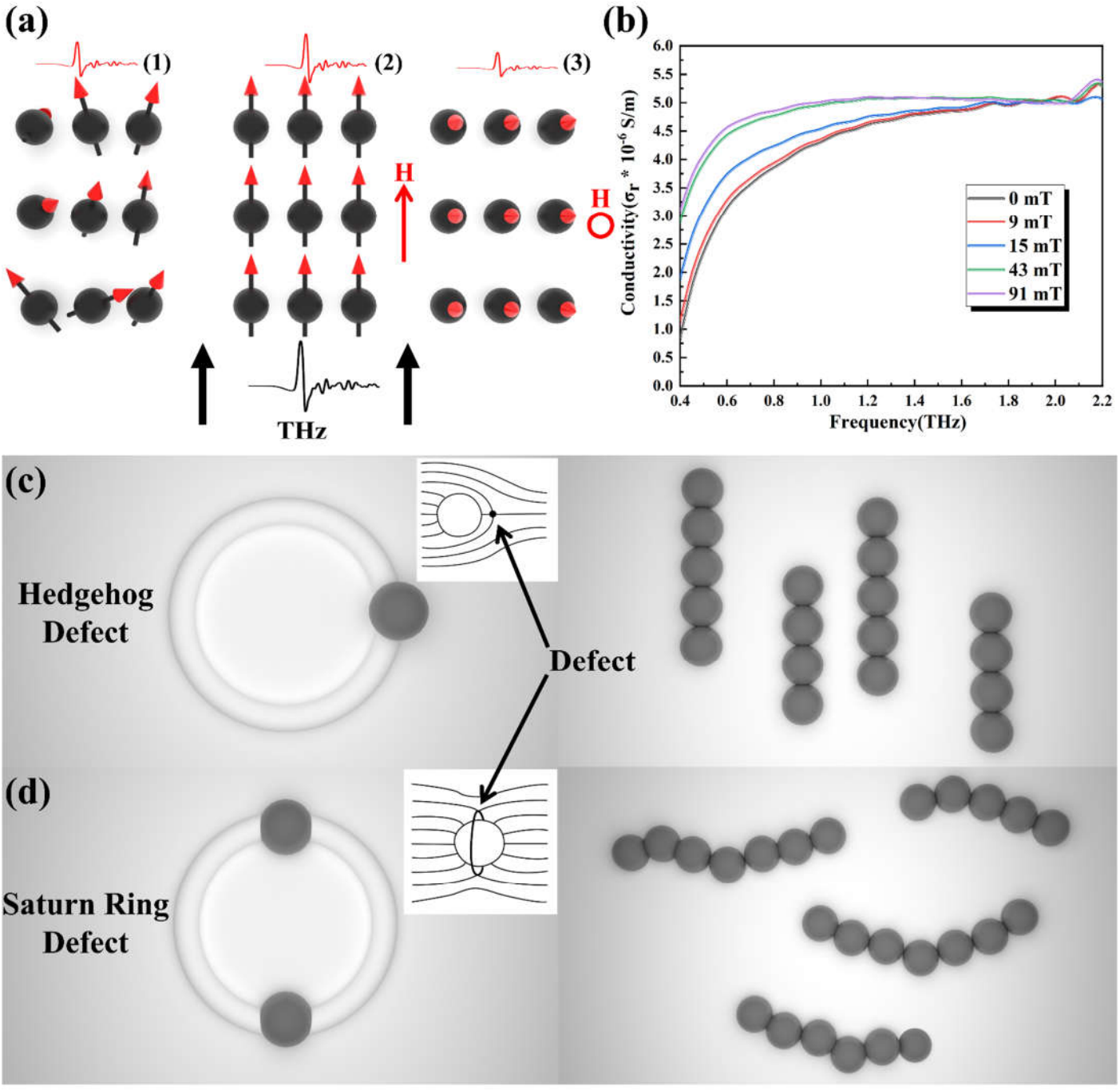

Figure 5. Schematic of THz modulation in magnetic fluid and FNLC. (a) The arrangement of Fe_3O_4 NPs under magnetic field and its effect on THz propagation. (1) NPs are randomly oriented and THz undergoes isotropic absorption. If the direction of the NPs is orthogonal (2)/parallel (3) to the THz electric field direction, the absorptivity will decrease/increase. (b) The real part of the magnetic fluid complex conductivity curve. (c) Schematic diagram of hedgehog defect. The interaction between colloids, which are bipolar and lead to linear chains. (d) Schematic diagram of Saturn ring defects. The interaction between colloids, which are quadrupolar and lead to zigzag chains.

Preprints (www.preprints.org) | NOT PEER-REVIEWED | Posted: 23 September 2022 doi:10.20944/preprints202209.0372.v1

After repeated experiments, the maximum MD of the magnetic fluid amplitude modulated THz wave is maintained in the range of 50%–55%. To enhance the MD, we propose the following strategy. To prepare FNLC, thermotropic nematic liquid crystal 5CB was doped into the magnetic fluid. When a liquid crystal, a material that has high birefringence, low absorption loss, and tunable properties through external fields in the THz band, is mechanically coupled to Fe_3O_4 NPs, the surface anchoring of the magnetic particles leads to the nematic ordered reconstruction of particles [36], increasing the weak magnetic interaction to a certain extent. This is mainly due to the extremely small elasticity coefficient of liquid crystals compared to solid-state materials, implying that topological defects can only extend to the size of a few atoms in a solid-state, but topological defects in liquid crystal can extend to tens of microns. When colloidal particles are doped into the nematic liquid crystal, the orientation of the nematic molecules is disturbed locally due to the interaction between the liquid crystal molecules and the surface of the colloidal particles. The disturbance propagates on the micro and nano-scale, which can be considered as an elastic deformation of the nematic liquid crystal. Topological defects will be induced when Fe_3O_4 NPs are dispersed in nematic liquid crystals. Saturn ring and Hedgehog defects can be observed under different anchoring conditions of magnetic particles. The mutual attraction of defects has the chain cluster effect of particles, implying that the dipole interaction of hedgehog defects causes Fe_3O_4 NPs to form linear chains, whereas the quadrupole interaction of Saturn ring defects forms zigzag chains (Figures 5(c) and 5(d)) [27]. This cluster effect induced by liquid crystal topological defects reduces the specific surface area of Fe_3O_4 NPs and enhances the Rayleigh scattering of THz waves, boosting their ability to modulate THz waves. The maximum MD increases to 78%.

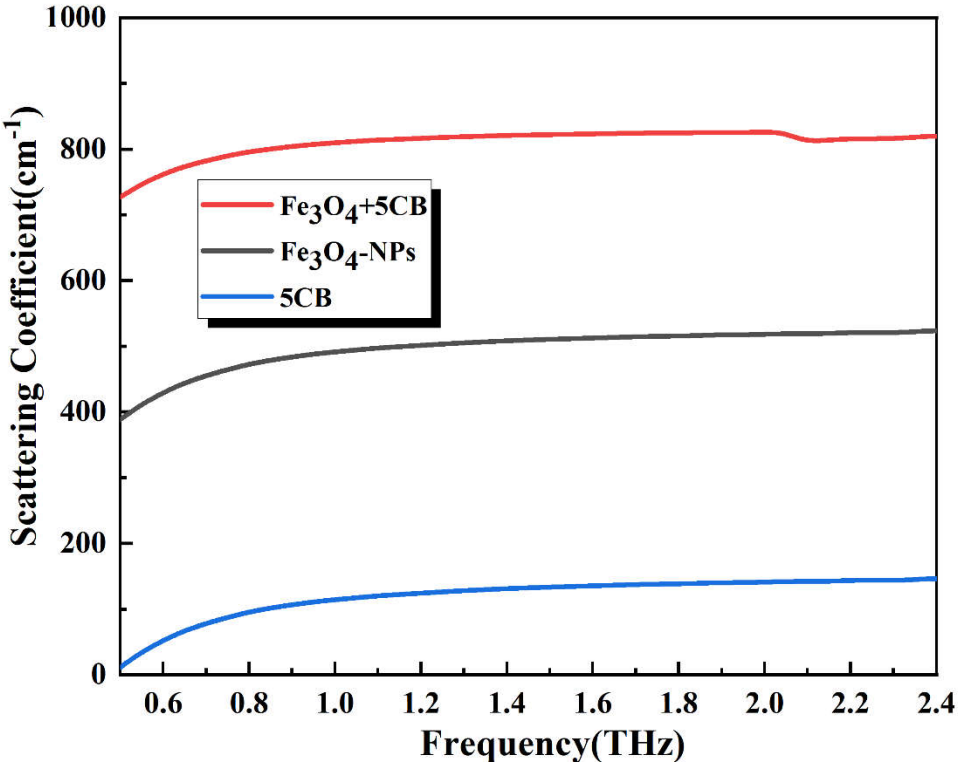

Figure 6. Scattering coefficient curve of 5CB, magnetic fluid and FNLC under 91 mT magnetic field.

To quantitatively illustrate the effect, we have calculated the scattering coefficient α_s of 5CB, magnetic fluid and FNLC under the action of 91 mT magnetic field based on the extended Lambert's law.

$$I = I_0 e^{-(\alpha_a + \alpha_s)l} \quad (1)$$

 doi:10.20944/preprints202209.0372.v1

where I represents the intensity of outgoing terahertz light, I_0 represents the intensity of incident terahertz light, α_a represents the absorption coefficient, α_s represents the scattering coefficient, and l represents the sample thickness. The calculated results are shown in Figure 6. After doping with liquid crystals, the scattering coefficient of the magnetic fluid increases significantly, indicating that the liquid crystal-induced chain cluster effect increases its ability to scatter THz waves and the ability of the magnetic fluid to modulate the amplitude of THz waves. This strategy, which is based on the resonant coupling of liquid crystal to magnetic particles, provides great potential for applications in actively tunable THz functional devices.

5. Conclusions

In this research, THz wave modulation properties of magnetic fluid and FNLC under the control of an external magnetic field were compared on the THz-TDS system using a self-made COC THz microfluidic chip. Both materials exhibit broadband modulation performance in the THz frequency range of 0.3–2.4, with a maximum MD of 54% for the magnetic fluid. After doping the magnetic fluid with the thermotropic nematic liquid crystal 5CB, the Fe_3O_4 NPs undergo a chain cluster effect because of the induction of liquid crystal topological defects, increasing the maximum MD of the amplitude of the THz waves to 78%. This strategy of doping thermotropic nematic liquid crystals to enhance the MO effect shows great potential for applications in THz filtering, modulation, and sensing.

Supplementary Materials: Figure S1: THz transmission spectrum of 2 mm thick COC material. Figure S2: Schematic diagram of phase sequence and structure of thermotropic molecules. Figure S3: THz frequency domain spectrum of a magnetic fluid at different magnetic field strength.

Author Contributions: Conceptualization, Q.H.M., B.S., and C.L.Z.; Methodology, Q.H.M. and B.S.; Validation, Q.H.M., X.Y.W., and S.Y.Q.; Formal Analysis, Q.H.M.; Investigation, Q.H.M., X.Y.W., B.P., B.Y.Z, H.Y.Z.; Writing–Original Draft, Q.H.M., and B.S.; Writing–Review & Editing, Q.H.M., and B.S.; Supervision, Q.H.M., B.S., and C.L.Z.; Resources, B.S., and C.L.Z.

Funding: Please add: This work was funded by the National Key R&D Program of China (Grant No .2021YFB3200100) and National Natural Science Foundation of China (NSFC) (61575131).

Data Availability Statement: The data presented in this study are openly available in Zenodo at https://doi.org/10.5281/zenodo.7036499.

Acknowledgments: The authors would like to thank Enago (www.enago.cn) for English language editing.

Conflicts of Interest: The authors declare no conflict of interest.

References

1. Gerken, F.; Posske, T.; Mukamel, S.; Thorwart, M., Unique Signatures of Topological Phases in Two-Dimensional THz Spectroscopy. *Phys Rev Lett* **2022**, *129(1)*, 017401. https://doi.org/10.48550/arXiv.2202.00030.
2. Zhu, S. Y.; Wu, G. B.; Pang, S. W.; Chan, C. H., Compact Terahertz Dielectric Folded Metasurface. *Advanced Optical Materials* **2021**, *10(3)* 2101663. https://doi.org/10.1002/adom.202101663.
3. Jing, R.; Shao, Y.; Fei, Z.; Lo, C. F. B.; Vitalone, R. A.; Ruta, F. L.; Staunton, J.; Zheng, W. J.; McLeod, A. S.; Sun, Z.; Jiang, B. Y.; Chen, X.; Fogler, M. M.; Millis, A. J.; Liu, M.; Cobden, D. H.; Xu, X.; Basov, D. N., Terahertz response of monolayer and few-layer WTe_2 at the nanoscale. *Nat Commun* **2021**, *12(1)*, 5594. https://doi.org/10.1038/s41467-021-23933-z.
4. Asgari, M.; Riccardi, E.; Balci, O.; De Fazio, D.; Shinde, S. M.; Zhang, J.; Mignuzzi, S.; Koppens, F. H. L.; Ferrari, A. C.; Viti, L.; Vitiello, M. S., Chip-Scalable, Room-Temperature, Zero-Bias, Graphene-Based Terahertz Detectors with Nanosecond Response Time. *ACS Nano* **2021**, *15*, 17966−17976. https://doi.org/10.1021/acsnano.1c06432.
5. Stantchev, R. I.; Li, K.; Pickwell-MacPherson, E., Rapid Imaging of Pulsed Terahertz Radiation with Spatial Light Modulators and Neural Networks. *ACS Photonics* **2021**, *8(11)*, 3150-3155. https://doi.org/10.1021/acsphotonics.1c00634.
6. Zhu, Y.; Liu, J.; Guo, T.; Wang, J. J.; Tang, X.; Nicolosi, V., Multifunctional $Ti_3C_2T_x$ MXene Composite Hydrogels with Strain Sensitivity toward Absorption-Dominated Electromagnetic-Interference Shielding. *ACS Nano* **2021**, *15(1)*, 1465-1474. https://dx.doi.org/10.1021/acsnano.0c08830.
7. Cao, Y.; Nallappan, K.; Xu, G.; Skorobogatiy, M., Add drop multiplexers for terahertz communications using two-wire waveguide-based plasmonic circuits. *Nat Commun* **2022**, *13(1)*, 4090. https://doi.org/10.1038/s41467-022-31590-z.
8. Wang, X. K.; Ye, J. S.; Sun, W. F.; Han, P.; Hou, L.; Zhang, Y., Terahertz near-field microscopy based on an air-plasma dynamic aperture. *Light Sci Appl* **2022**, *11(1)*, 129. https://doi.org/10.1038/s41377-022-00822-8.
9. Yang, K.; Chopra, N.; Abbasi, Q. H.; Qaraqe, K. A.; Alomainy, A., Collagen Analysis at Terahertz Band Using Double-Debye Parameter Extraction and Particle Swarm Optimisation. *IEEE Access* **2017**, *5*, 27850-27856. https://doi.org/10.1109/ACCESS.2017.2674520.
10. Zhang, Z.; Guo, X.; Yang, M.; Yang, Q.; Yan, X.; Liang, L.; Liu, L.; Yao, J., Time-frequency joint mappings of a terahertz metasurface for multi-dimensional analysis of biological cells. *Opt Lett* **2022**, *47(15)*, 3704-3707. https://doi.org/10.1364/OL.464443.
11. You, X.; Wang, C.-X.; Huang, J.; Gao, X.; Zhang, Z.; Wang, M.; Huang, Y.; Zhang, C.; Jiang, Y.; Wang, J.; et.al., Towards 6G wireless communication networks: vision, enabling technologies, and new paradigm shifts. *Science China Information Sciences* **2020**, *64(1)*, 1-74. https://doi.org/10.1007/s11432-020-2955-6.
12. Seifert, T.; Jaiswal, S.; Martens, U.; Hannegan, J.; Braun, L.; Maldonado, P.; Freimuth, F.; Kronenberg, A.; Henrizi, J.; Radu, I.; Beaurepaire, E.; Mokrousov, Y.; Oppeneer, P. M.; Jourdan, M.; Jakob, G.; Turchinovich, D.; Hayden, L. M.; Wolf, M.; Münzenberg, M.; Kläui, M.; Kampfrath, T., Efficient metallic spintronic emitters of ultrabroadband terahertz radiation. *Nature Photonics* **2016**, *10(7)*, 483-488. https://doi.org/10.1038/NPHOTON.2016.91.
13. Tan, T. C.; Srivastava, Y. K.; Ako, R. T.; Wang, W.; Bhaskaran, M.; Sriram, S.; Al-Naib, I.; Plum, E.; Singh, R., Active Control of Nanodielectric-Induced THz Quasi-BIC in Flexible Metasurfaces: A Platform for Modulation and Sensing. *Adv Mater* **2021**, *33(27)*, e2100836. https://doi.org/10.1002/adma.202100836.
14. Sun, J.; Zheng, Y.; Shi, J.; Zhao, Y.; Li, Y.; Wu, D.; Cai, H.; Zhang, X.; Zhu, X.; Liu, Y.; Sun, X.; Chao, Z.; Yin, H.; Lu, W.; Ding, H., Propagation characteristics of terahertz wave in inductively coupled plasma. *Opt Express* **2021**, *29(22)*, 35837-35847. https://doi.org/10.1364/OE.435910.
15. Fan, F.; Chen, S.; Chang, S.-J., A Review of Magneto-Optical Microstructure Devices at Terahertz Frequencies. *IEEE Journal of Selected Topics in Quantum Electronics* **2017**, *23(4)*, 1-11. https://doi.org/10.1109/JSTQE.2016.2537259.
16. Xiong, L.-Y.; Zhang, B.; Ji, H.-Y.; Wang, W.; Liu, X.; He, S.-L.; Shen, J.-L., Active Optically Controlled Broadband Terahertz Modulator Based on Fe_3O_4 Nanoparticles. *IEEE Transactions on Terahertz Science and Technology* **2018**, *8(5)*, 535-540. https://doi.org/10.1109/TTHZ.2018.2853991.
17. Shalaby, M.; Peccianti, M.; Ozturk, Y.; Al-Naib, I.; Hauri, C. P.; Morandotti, R., Terahertz magnetic modulator based on magnetically clustered nanoparticles. *Applied Physics Letters* **2014**, *105(15)*. https://doi.org/10.1063/1.4898095.
18. Liu, X.; Xiong, L.; Yu, X.; He, S.; Zhang, B.; Shen, J., Magnetically controlled terahertz modulator based on Fe_3O_4 nanoparticle ferrofluids. *Journal of Physics D: Applied Physics* **2018**, *51(10)*. https://doi.org/10.1088/1361-6463/aaab97.
19. Shrekenhamer, D.; Chen, W. C.; Padilla, W. J., Liquid crystal tunable metamaterial absorber. *Phys Rev Lett* **2013**, *110(17)*, 177403. https://doi.org/10.1103/PhysRevLett.110.177403.
20. Minovich, A.; Farnell, J.; Neshev, D. N.; McKerracher, I.; Karouta, F.; Tian, J.; Powell, D. A.; Shadrivov, I. V.; Hoe Tan, H.; Jagadish, C.; Kivshar, Y. S., Liquid crystal based nonlinear fishnet metamaterials. *Applied Physics Letters* **2012**, *100(12)*. https://doi.org/10.1063/1.3695165.
21. Chen, C. C.; Chiang, W. F.; Tsai, M. C.; Jiang, S. A.; Chang, T. H.; Wang, S. H.; Huang, C. Y., Continuously tunable and fast-response terahertz metamaterials using in-plane-switching dual-frequency liquid crystal cells. *Opt Lett* **2015**, *40(9)*, 2021-4. http://dx.doi.org/10.1364/OL.40.002021.
22. Savo, S.; Shrekenhamer, D.; Padilla, W. J., Liquid Crystal Metamaterial Absorber Spatial Light Modulator for THz Applications. *Advanced Optical Materials* **2014**, *2(3)*, 275-279. https://doi.org/10.1002/adom.201300384.

23. Isić, G.; Vasić, B.; Zografopoulos, D. C.; Beccherelli, R.; Gajić, R., Electrically Tunable Critically Coupled Terahertz Metamaterial Absorber Based on Nematic Liquid Crystals. *Physical Review Applied* **2015**, *3(6)*, 064007. https://doi.org/10.1103/PhysRevApplied.3.064007.
24. J, J. P.; Shalini, M.; Patel, N.; Sarawade, P.; S, R., Thermo optical study of nematic liquid crystal doped with ferrofluid. *AIP Conference Proceedings* **2017**, *1837*, 040066. https://doi.org/10.1063/1.4982150.
25. Huang, H.; Shao, S.; Wang, G.; Ye, P.; Su, B.; Zhang, C., Terahertz spectral properties of glucose and two disaccharides in solid and liquid states. *iScience* **2022**, *25(4)*, 104102. https://doi.org/10.1016/j.isci.2022.104102.
26. Wang, J.-H.; Wang, G.-Y.; Liu, X.; Shao, S.-Y.; Huang, H.-Y.; Ding, C.-X.; Su, B.; Zhang, C.-L., Effect of external electric field on the terahertz transmission characteristics of electrolyte solutions. *Chinese Physics B* **2022**, *30(11)*, 110204. https://doi.org/10.1088/1674-1056/abff24.
27. Dierking, I.; Yoshida, S.; Kelly, T.; Pitcher, W., Liquid crystal-ferrofluid emulsions. *Soft Matter* **2020**, *16(26)*, 6021-6031. https://doi.org/10.1039/d0sm00880j.
28. Fernandes, P. R. G.; Mukai, H.; Laczkowski, I. M., Magneto-optical effect in lyotropic liquid crystal doped with ferrofluid. *Journal of Magnetism and Magnetic Materials* **2005**, *289*, 115-117. https://doi.org/10.1016/j.jmmm.2004.11.034.
29. Melle, S.; Rubio, M. A.; Fuller, G. G., Time scaling regimes in aggregation of magnetic dipolar particles: scattering dichroism results. *Phys Rev Lett* **2001**, *87(11)*, 115501. https://doi.org/115501.10.1103/PhysRevLett.87.115501.
30. Dorney, T. D.; Baraniuk, R. G.; Mittleman, D. M., Material parameter estimation with terahertz time-domain spectroscopy. *J. Opt. Soc. Am. A* **2001**, *18(7)*, 1562-71. https://doi.org/10.1364/JOSAA.18.001562.
31. Zhao, P.; Shi, L.; Liu, Y.; Wang, Z.; Pu, S.; Zhang, X., Iron-oxide nanoparticles embedded silica microsphere resonator exhibiting broadband all-optical wavelength tunability. *Opt Lett* **2014**, *39(13)*, 3845-8. http://dx.doi.org/10.1364/OL.39.003845.
32. Bertasius, P.; Macutkevic, J.; Banys, J.; Gaidukovs, S.; Barkane, A.; Vaivodiss, R., Synergy effects in dielectric and thermal properties of layered ethylene vinyl acetate composites with carbon and Fe_3O_4 nanoparticles. *J. APPL. POLYM. SCI.* **2019**, *137(24)*, 48814. https://doi.org/10.1002/APP.48814.
33. Chen, S.; Fan, F.; Chang, S.; Miao, Y.; Chen, M.; Li, J.; Wang, X.; Lin, L., Tunable optical and magneto-optical properties of ferrofluid in the terahertz regime. *Opt Express* **2014**, *22(6)*, 6313-6321. https://doi.org/6313-21.10.1364/OE.22.006313.
34. Scholten; P., The origin of magnetic birefringence and dichroism in magnetic fluids. *IEEE Transactions on Magnetics* **1980**, *16(2)*, 221-225. https://doi.org/10.1109/TMAG.1980.1060595.
35. Zu, P.; Chan, C. C.; Siang Lew, W.; Jin, Y.; Fen Liew, H.; Chang Wong, W.; Dong, X.; Zhan Foo, C., Laser self-induced tunable birefringence of magnetic fluid. *Applied Physics Letters* **2013**, *102(18)*, 181116. http://dx.doi.org/10.1063/1.4804579.
36. Walton, D.; Shibli, S. M., Effect of the liquid crystal occur environment on the aggregation of magnetic grains in ferronematics. *Journal of Magnetism and Magnetic Materials* **2004**, *279(2-3)*, 283-288. http://dx.doi.org/10.1016/j.jmmm.2003.12.1424.